11

Fault Branching and Long-Term Earthquake Rupture Scenario for Strike-Slip Earthquakes

Yann Klinger, Jin-Hyuck Choi, and Amaury Vallage

ABSTRACT

Careful examination of surface rupture for large continental strike-slip earthquakes reveals that for the majority of earthquakes, at least one major branch is involved in the rupture pattern. Often, branching might be either related to the location of the epicenter or located toward the end of the rupture, and possibly related to the stopping of the rupture. In this work, we examine three large continental earthquakes that show significant branches and for which ground surface rupture has been mapped in great details. In each case, rupture conditions are described, including dynamic parameters, past earthquakes history, and regional stress orientation, to see if the dynamic stress field would a priori favor branching. In one case, we show that it was not the first time that an earthquake was branching in a similar fashion. Long-term geomorphology hints at the existence of a strong asperity in the zone where the rupture branched off the main fault. There, no evidence of throughgoing rupture could be seen along the main fault, while the branch is well connected to the main fault. This set of observations suggests that for specific configurations, some rupture scenarios involving systematic branching are more likely than others.

11.1. INTRODUCTION

Surface ruptures associated with large continental earthquakes bring a wealth of information about rupture processes and fault structures [i.e., *Haeussler et al.*, 2004; *King et al.*, 2005; *Xu et al.*, 2006; *Wei et al.*, 2011; *Teran et al.*, 2015]. Until the late 80s, however, the potential of such information was not well recognized and details of surface ruptures during an earthquake were often poorly documented. Indeed, surface ruptures for large events are distributed over tens to hundreds of kilometers, depending on the magnitude of the event, making them difficult to be comprehended when one is limited only to field observation and/or to low-resolution aerial photos. In addition, earthquake source studies are mostly focused on teleseismic distances, which limits the frequency domain addressed to be close to 1 Hz at most. Such frequency domain, 1 Hz and lower, corresponds to a resolution of a few kilometers at best, which is out of scale when compared to details of the rupture geometry seen during field survey. Less often, waveform inversion is carried out at higher frequency, allowing for a more detailed view of the seismic source at smaller scale [*Kim and Dreger*, 2008; *Ji et al.*, 2015].

Major improvements in remote sensing during the last two decades have opened new avenues to study details of surface rupture geometry and to build a corpus of homogeneous data to feed more and more efficient modeling tools. In 1992, the Mw 7.3 Landers earthquake was the first large earthquake for which the deformation field was imaged at once [*Massonnet et al.*, 1993]. In parallel, the Landers earthquake was also one of the first large events that were mapped at a very detailed scale over its entire length [*Sieh et al.*, 1993], thanks to excellent exposures and proximity of research centers. From the early 2000s,

Institut de Physique du Globe de Paris, Université Sorbonne Paris Cité, Université Paris Diderot, Paris, France

Fault Zone Dynamic Processes: Evolution of Fault Properties During Seismic Rupture, Geophysical Monograph 227, First Edition. Edited by Marion Y. Thomas, Thomas M. Mitchell, and Harsha S. Bhat.

the availability of new submetric optical satellites and topography to civilian scientists increased the resolution by one order of magnitude. This has allowed scientists to investigate more thoroughly major continental ruptures around the world, without being constrained by the size of the rupture [i.e., *Klinger et al.*, 2005; *Li et al.*, 2005], including revisiting past large events [*Klinger et al.*, 2011; *Ren et al.*, 2016]. This improvement in image resolution and topography also helped with mapping active faults in general, contributing to a better knowledge of the surficial geometry of continental faults. Hence, over the last two decades scientists have been building data sets of surface rupture maps [*Wesnousky*, 2008; *Klinger*, 2010] with an increasing level of details, often down to a few meters or better, including revisiting past events and some of the old archived aerial photos. The number of events currently well documented is about 20 to 30, depending on the level of details needed.

The main outcome of this improvement in mapping ruptures has been to bring forward the fact that for continental earthquakes, at least, complexity of earthquake source and associated ground rupture is the general rule rather than the exception. Most of the recently documented earthquakes have proven to have complex ruptures to some extent, with significant fault segmentation and jogs, such as the 2001 Kunlun earthquake [*Klinger et al.*, 2005] or the 1999 Izmit-Duzce sequence [*Lettis et al.*, 2000], and several active branches such as the 2002 Denali earthquake [*Haeussler et al.*, 2004] or the 2010 El-Mayor earthquake [*Wei et al.*, 2011; *Oskin et al.*, 2012], to name only a few. In fact, complexity appears at all scales, from cracks at the metric scale, to kilometric-long branches [*Vallage et al.*, 2015]. Fault segmentation characterizing the complexity of the overall fault geometry on a larger scale (tens of kilometers) seems to be persistent over successive seismic cycles, although the details of geometry for individual fault segments could be modified during individual earthquakes [*Klinger*, 2010]. The relay zones that link segments, especially for strike-slip faults, have been regarded as playing a special role in initiation and arrest of earthquake ruptures [*Wesnousky*, 2006], related to the ill-configuration of local fault geometry that hinders efficient accommodation of the stress accumulated during the interseismic period [*King and Nabelek*, 1985]. Eventually, at the end of an earthquake rupture, the residual stress would be higher at jogs, compared to geometrically simpler fault segments, and more prone to initiate new ruptures [*Nielsen and Knopoff*, 1998; *Duan and Oglesby*, 2006].

Since the geometrical complexity appears to be an inherent characteristic of the fault structure, many studies have been conducted to explore the impact of the fault geometry on rupture dynamic processes. Indeed, geological observations remain difficult to include directly in rupture models, as they often show a level of detail that is still beyond computational capabilities of state-of-the-art models. Hence, through simplified models, most often addressing the geometry in 2D, the effects of jogs, fault branching, or damage, in conjunction with local stress orientation and rupture speed, have been systematically explored [*Harris and Day*, 1993; 1999; *Poliakov et al.*, 2002; *Kame et al.*, 2003; *Thomas et al.*, 2017 (this volume)], as well as impact of fault geometry on evaluating various rupture scenario for specific fault systems [e.g., *Muller and Aydin*, 2004]. These seminal works show that earthquake rupture patterns and earthquake cycle can probably not be well understood if fault geometry is not properly taken into account [*Bhat et al.*, 2004; *Bhat et al.*, 2007; *Elliott et al.*, 2015].

Some of the geometrical asperities can be kilometric in size. More specifically, during several earthquakes it has been shown that the existence of large branches had affected the course of the rupture process significantly, in diverting the rupture propagation from what would be considered the long-term geological trace of the fault, as discussed further in coming sections of this chapter. These branches, however, because they are large-scale features well visible in the landscape, have to be long-lived features and could not be activated only during a single event. Hence, in the next sections we explore three pathological cases where large-scale branches were involved during large continental strike-slip ruptures. The three cases presented are the 1905 M8 Bolnay event, the 2002 Mw 7.9 Denali event, and the 2001 Mw 7.8 Kunlun event. For the Bolnay and the Kunlun earthquakes, new high-resolution maps of the surface rupture, focused on the location where branches are joining the main rupture, are presented. These maps are based on submetric satellite images, complemented with field observations. Special care has been taken when mapping to document secondary deformations that are likely relevant to the understanding of earthquake-rupture branching processes. Data for the Denali earthquake are solely derived from published literature. In the case of the Bolnay earthquake, although preservation of the landform is exceptional due to very limited erosion, it could not be excluded that some secondary cracks are not visible anymore, as images were acquired about a century after the event. In the case of the Kunlun event, images were acquired in the year following the event, and maps established from satellite imagery appear to be complete down to metric scale features, when compared with field observations [*Klinger et al.*, 2005]. In each case, we present the geometry of the rupture in detail and show how the rupture proceeded through the branching section. Eventually, in one case we present evidence suggesting that branching observed during the last event might have happened similarly during previous events. If this would be the case, then better understanding of the condition leading to such persistent branching, as well as fault geometry, would allow the building of rupture scenarios with a more limited range of possible scenarios [*Schwartz et al.*, 2012; *Mignan et al.*, 2015].

11.2. CASE STUDIES

11.2.1. The 1905 M8 Bolnay Earthquake, Mongolia

In 1905, a series of earthquakes struck northwestern Mongolia with two M~8 earthquakes 14 days apart. The Tsetserleg M8 earthquake occurred on 9 July 1905 and the Bolnay M8+ event on 23 July 1905. This sequence is one of the largest continental earthquake sequences known. These earthquakes broke faults that relate to the northern most extent of the India-Eurasia collision [*Tapponnier and Molnar*, 1977]. Both earthquakes were dominated by strike-slip mechanisms. Several works have already addressed some details of the surface rupture, seismological aspects, or triggering issues for these two events [*Khilko et al.*, 1985; *Baljinnyam et al.*, 1993; *Chéry et al.*, 2001; *Schlupp and Cisternas*, 2007; *Choi et al.*, 2015; *Rizza et al.*, 2015] that will not be repeated here. Focus will be limited here to aspects more specifically related to branching during the rupture process of the second event, the Bolnay earthquake. No obvious branches were documented for the Tsetserleg event, although its surface rupture displays some degree of geometrical complexity, including significant changes of azimuth along the rupture path [*Choi et al.*, 2015].

The Bolnay rupture is formed by a main E-W rupture, about 385 km long, where strike-slip dominates the deformation style. The left-lateral surface slip averages 6 m with a maximum surface slip about 10.6 m, documented 200 km east of the epicenter. A major 80 km long branch, the Teregtiyn fault, is associated with the main rupture (Figure 11.1). This branch is itself divided into two sections 15 km long and 65 km long respectively. The Teregtiyn fault strikes N140E, making an angle of 44° with the main rupture (Figure 11.1). Displacement along the Teregtiyn branch is mostly characterized by right-lateral strike-slip, kinematically consistent with the left-lateral motion along the main rupture, with some thrust component along the closest section to the main rupture. Horizontal slip is about 1 m to 3 m, and thrust motion reaches 1.3 m on average. For the sake of completeness, the Dungen fault should also be mentioned. It is oriented N-S, about 90° from the main rupture. This fault, located about 100 km eastward from the epicentral area, is about 35 km long. Ground surface ruptures are characterized by a series of right-lateral en-echelon cracks with no obvious primary fault plane. At this stage it is impossible to assess the existence of a fully connected fault plane even at depth. This part of the rupture is actually not connected to the main Bolnay rupture, and although it is classically associated with the rupture of the Bolnay earthquake [*Schlupp and Cisternas*, 2007], the timing of the rupture remains arguable, and it could be associated with the Tsetserleg event as well. In any case, this branch does not seem to have influenced the rupture pattern of the Bolnay earthquake significantly, and it will not be discussed further here.

The Bolnay event typifies events where the epicenter is located at the junction point between the main rupture and a major branch. Although uncertainty about epicentral location due to scarcity of records impedes more precision, seismic source inversion [*Schlupp and Cisternas*, 2007] suggests that the rupture might have actually started at the northern end of the Teregtiyn branch, triggering bilateral rupture along the main fault trace, from the junction point. During the same time, part of the rupture also propagated southward along the Teregtiyn fault. Both faults have a long-term imprint in the topography that denotes that they have been active for quite some time. Cumulative offsets along the Teregtiyn, however, are smaller with a maximum documented value of 16.5 m, which confirms that this fault

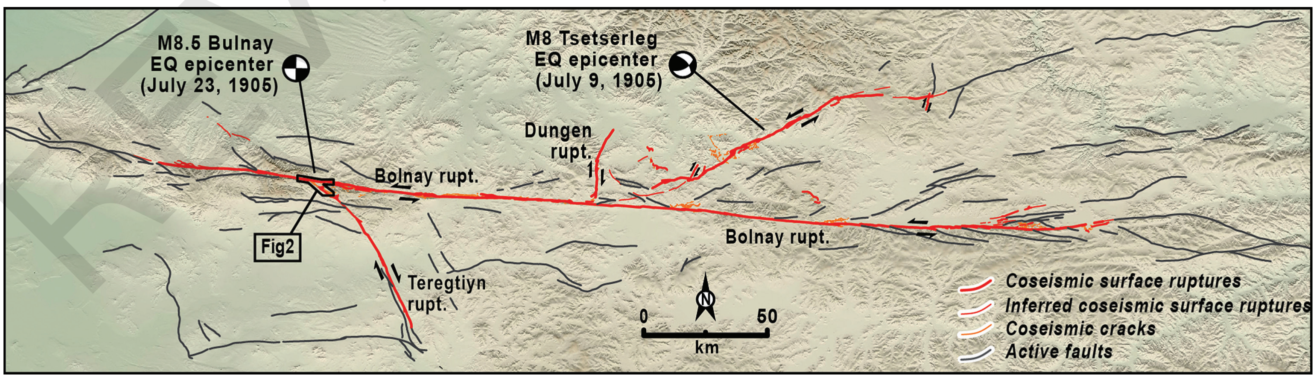

Figure 11.1 General rupture map of the 1905 earthquake sequence in Mongolia, including both the Tsetserleg and the Bolnay earthquakes. The epicenter of the Bolnay rupture is located in the area where the Teregtiyn fault connects to the main Bolnay fault. *See electronic version for color representation*.

is a secondary structure, not necessarily activated every time the main Bolnay fault breaks. Mapping of the 1905 surface rupture reveals that the two faults do not join through a triple junction characterized by simple well-defined fault traces (Figure 11.2). Instead, the exact location of the junction is characterized by a maze of cracks mostly located in the inner corner between the two fault strands. Outside of this zone, damage is limited to a few cracks oriented according to the fabric of the local geology. Many cracks, including the structures bounding the area to the south, are mainly showing evidence of extension, in agreement with the local kinematic controlled by simultaneous activation of the left-lateral Bolnay fault and the right-lateral Teregtiyn segment. Indeed, the pattern of rupture illustrates that such junction could not be stable over long periods of time, and fault geometry at that location has to reconfigure itself during each event to accommodate negative volumetric change.

11.2.2. The 2002 Mw 7.9 Denali Earthquake, Alaska

On 3 November 2002, the Mw 7.9 Denali earthquake broke 340 km of the central part of the Denali fault (Figure 11.3) in Alaska, USA [*Haeussler et al.*, 2004].

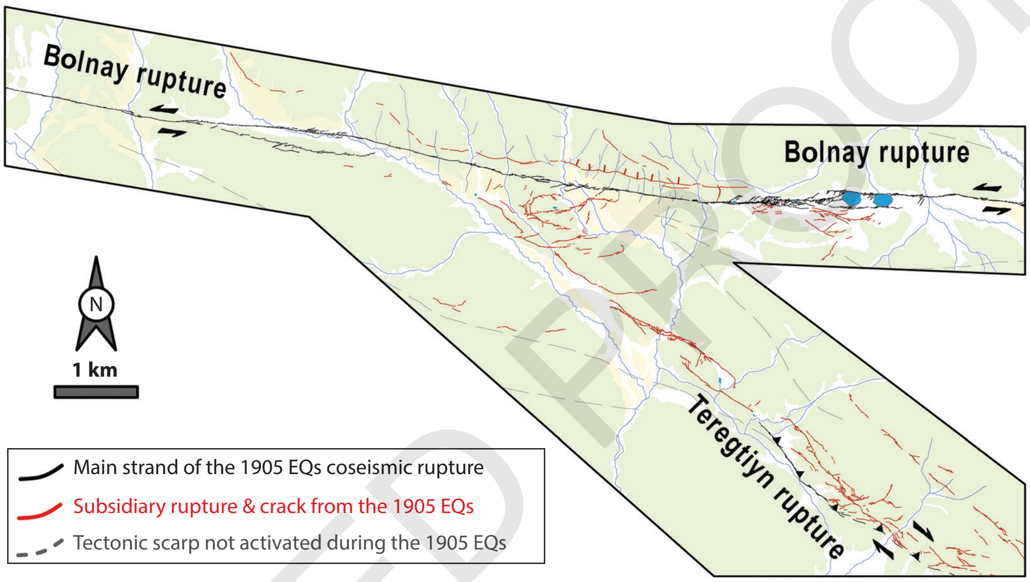

Figure 11.2 Detail of the rupture pattern associated with the 1905 Bolnay earthquake, derived from satellite imagery analyses and field observations. The corner in-between the Bolnay rupture and the Teregtiyn branch appears to be significantly shattered by randomly oriented cracks. *See electronic version for color representation*.

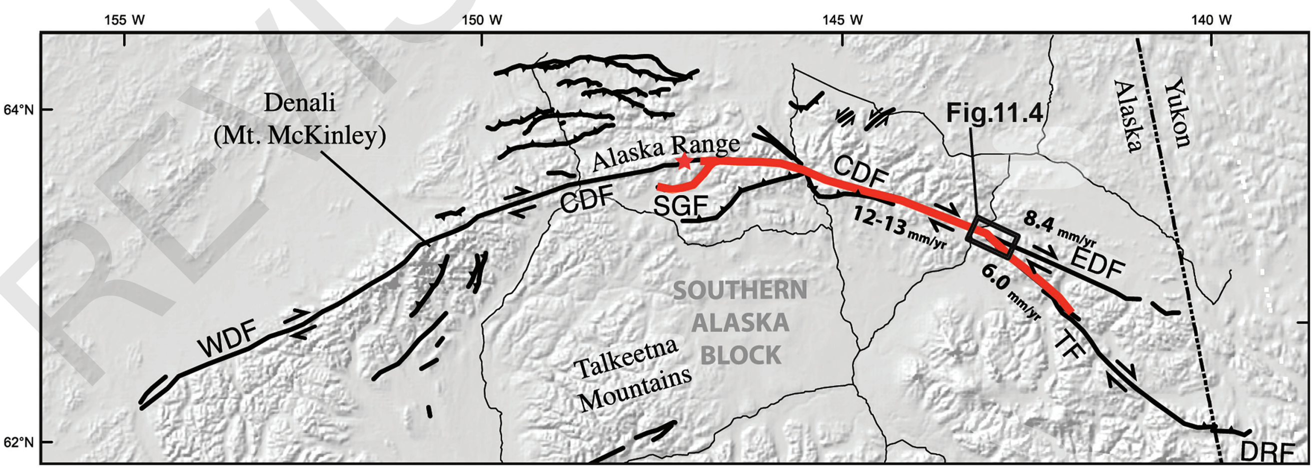

Figure 11.3 General rupture map of the 2002 Denali rupture (in red) and of the Denali fault system. CDF = Central Denali fault, EDF = East Denali fault, WDF = West Denali fault, SGF = Susitna Glacier fault, TF = Totschunda fault. Adapted from *Schwartz et al.* [2012]. *See electronic version for color representation*.

This fault is part of the complex fault system that accommodates the collision between the Yakuta block and the North America block [*Elliott et al.*, 2010] through a partitioned tectonic system [*Vallage et al.*, 2014], where the Denali fault acts as a major right-lateral strike-slip fault. The long-term slip rate along the central part of the Denali fault is about 12 ± 3 mm/yr [*Matmon et al.*, 2006; *Mériaux et al.*, 2009].

The rupture initiated along the Susitna Glacier fault segment, a thrust fault that was unrecognized before the 2002 earthquake [*Haeussler et al.*, 2004]. After 48 km, this thrust fault connects to the central Denali fault, where the rupture developed as a pure strike-slip rupture for about 225 km, before branching onto the Totschunda fault, where it ruptured 66 km additional kilometers (Figure 11.4). On average, the horizontal motion was 4.5 m to 5 m with a reported maximum of 8.8 m [*Haeussler et al.*, 2004]. The average right-lateral horizontal slip along the Totschunda segment is 1.7 m. Seismological records suggest that part of the rupture went super-shear in the central section, although it was only along a limited section that ended even before the rupture approached the junction between the proper Denali fault and the Totschunda fault branch [*Dreger et al.*, 2004; *Dunham and Archuleta*, 2004].

The reason why the Denali rupture branched on the Totschunda fault has been widely discussed. Coming from the west along the Denali fault, at 62.82°N, 143.35°W the Denali fault splits into two strands, the eastern Denali fault to the north and the Totschunda fault to the south. Each strand accommodates about half of the total slip rate of the Denali fault [*Matmon et al.*, 2006]. Although the full fault geometry is not yet well understood, the two strands get back together about 250 km farther south into a single Denali fault [*Spotila and Berger*, 2010]. Recent observations suggest that along the eastern Denali section, soon after the junction, the strike-slip component of the Denali fault becomes very small and that the fault is currently dominated by dip-slip motion [*Marechal*, 2015]. Most of the strike-slip component would then be accommodated along the Totschunda strand [*Marechal et al.*, 2015]. In the field, however, the morphological trace of each segment can be followed to the exact junction point (Figure 11.4), suggesting that both segments have been active during the Late Quaternary. *Schwartz et al.* [2012], based on paleoseismological findings, argue that according to the timing of the last earthquake on each strand, it was more favorable for an earthquake rupture propagating eastward to continue along the Totschunda fault rather than along the eastern Denali fault; the accumulated slip-deficit since the last event on the east Denali fault would be somewhere between 0.62 m and 3.65 m, whereas the accumulated slip-deficit along the Totschunda fault would stand somewhere between 2.77 m and 5.29 m. Hence, for these authors, there was no need to invoke any additional processes to explain the branching of the Denali rupture. Conversely, several studies have considered more specifically the local stress conditions [*Dreger et al.*, 2004] and the effect of dynamic propagation of the rupture during the Denali earthquake [*Bhat et al.*, 2004] as the main causes for branching. In fact, the Totschunda branch is

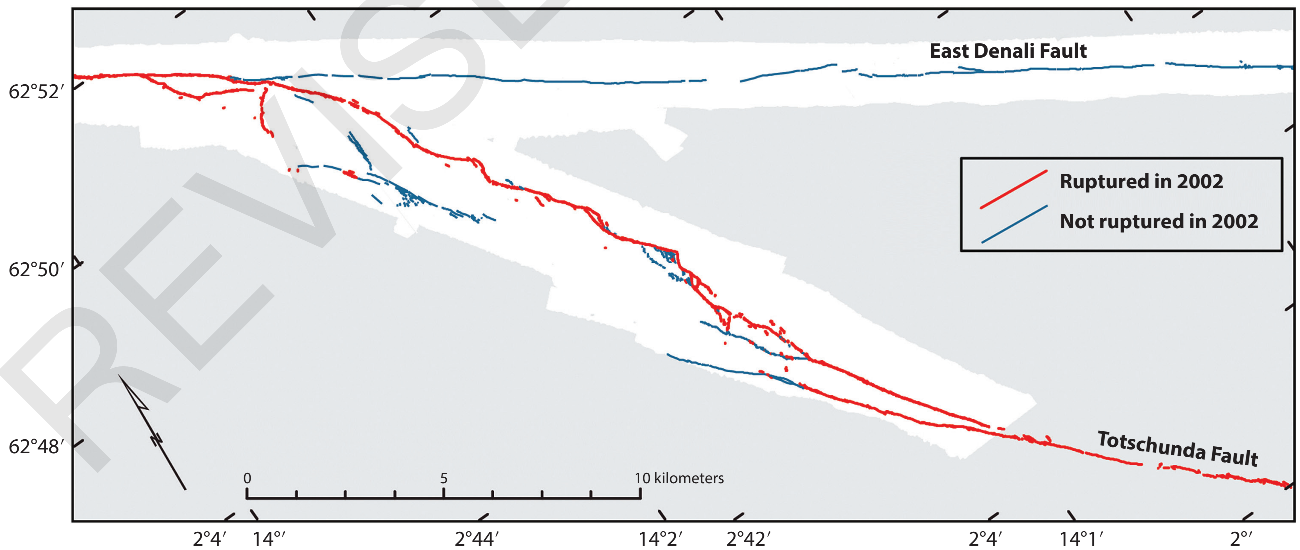

Figure 11.4 Detail from Figure 11.3. Area where the Totschunda fault branches off from the Eastern Denali fault strand. The two fault systems appear to be well connected and the 2002 Denali rupture (in red) is very continuous across the junction. After *Schwartz et al.* [2012]. *See electronic version for color representation*.

located in the extensional quadrant of the central Denali fault and is naturally prone to rupture when dynamically loaded by a seismic rupture coming from west [*Kame et al.*, 2003], independently of the rupture speed. Hence, because the uncertainties on dating past earthquakes along the Denali fault and the Totschunda fault remain large, no definitive conclusion can be drawn from paleoseismic data alone. Also, it is difficult at this stage to ascertain that dynamic rupture effect is the only reason the rupture branched, it is clear that it could have only helped.

11.2.3. The 2001 Mw 7.8 Kunlun Earthquake, China

On 14 November 2001, the Kunlun earthquake, also coined the Kokoxili earthquake, broke 430 km of the Kunlun fault. The moment magnitude for this event, dominated by left-lateral strike-slip, is Mw 7.8. The Kunlun fault counts as one of the largest continental strike-slip faults to participate in the eastward extrusion of Tibet, in the context of the continental collision between the Indian plate and the Eurasian plate [*Tapponnier and Molnar*, 1977]. The Kunlun fault is about 1500 km long, with a finite offset estimated to be about 150 km [*Van Der Woerd et al.*, 2000]. Slip rates at different time scales have been estimated along this fault; along the western section of the fault, which is of concern here, both geodetic and long-term geologic slip rates point to values about 10 mm/yr ± 2 mm/yr [*Wang et al.*, 2001; *Van Der Woerd et al.*, 2002; *Li et al.*, 2005]. The Kunlun fault is segmented at a different spatial scale; at a scale of hundreds of kilometers, the fault is characterized by sections with significant differences (>5°) in azimuth that translate into some dip-slip component, in addition to the dominant strike-slip motion. For example, the Xidatan section, located directly east of the Kunlun rupture, is characterized by a slight opening component in addition to the lateral motion to accommodate the ~10° azimuth difference between the two successive fault sections. This first-order structuration of the fault is most probably related to the existence of an older suture zone, associated with the progressive buildup of the Tibetan plateau [*Tapponnier et al.*, 2001], that guided the early localization of the deformation during the more recent emplacement of the strike-slip fault. The fault appears also to be segmented at a smaller scale of 10 km to 20 km. Structural discontinuities, such as relay zones, bends, and joining side faults can be found along the 2001 earthquake surface rupture. These coincide with strong variation in the coseismic slip distribution and were interpreted as evidence of such segmentation [*Klinger et al.*, 2006; *Klinger*, 2010].

The Kunlun earthquake rupture was unilateral [*Vallee et al.*, 2008]. The rupture initiated in a small pull-apart basin and after going through an oblique normal fault section, it fully developed along the Kusai segment, over ~270 km (Figure 11.5). Then the rupture branched southward on the so-called Kunlun Pass fault, where the rupture propagated for an extra 70 km before dying out, leaving the Xidatan segment, the long-term continuation of the Kunlun fault, unbroken. Along the eastern section of the Kunlun Pass fault, in addition to the strike-slip motion, a significant thrust component was observed with the fault dipping to the north [*Klinger et al.*, 2005]. Detailed measurements of the rupture velocity along the Kusai segment and the Kunlun Pass fault show that along a significant part of the Kusai segment the rupture went super-shear [*Bouchon and Vallée*, 2003; *Vallee et al.*, 2008]. Eventually, the rupture slowed down at the branching point that corresponds to a change of azimuth of about 5° southward along the rupture. The horizontal slip, after a progressive increase of up to ~6 m when approaching the branching point location from the west, dropped abruptly to less than 2 m at the fault junction. Such asymmetric slip profile is often associated with fault asperities [*Manighetti et al.*, 2004; *Klinger et al.*, 2006], which would also be consistent with the brutal slow down of the rupture propagation.

The seismological history of the Xidatan section, the long-term continuation of the Kunlun fault east of the Kusai section, is not well established yet. The morphology

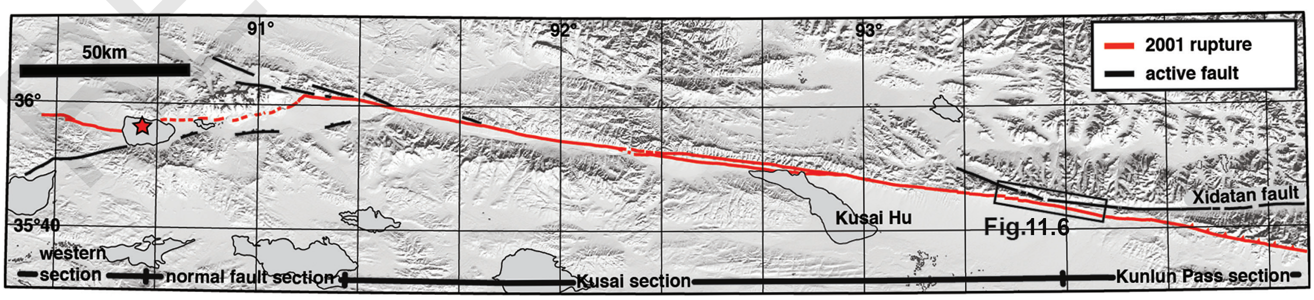

Figure 11.5 Rupture map of the Mw 7.8 2001 Kunlun earthquake. The red star marks the epicenter location. The rupture went unilaterally and ended on the Kunlun Pass fault, leaving the Xidatan section unbroken. After *Klinger et al.* [2005]. *See electronic version for color representation.*

of the fault along this segment is rather smooth, and the few available dates from undeformed alluvial surfaces and paleoseismological trenches suggest that no earthquake has occurred along this segment during the last 280 years [*Van Der Woerd et al.*, 2002], although one earthquake probably occurred along the Xidatan section during the last 600 years [*Lin et al.*, 2006; *Klinger et al.*, 2015]. Along the Xidatan segment, as well as along the Kusai segment, few evidence for past earthquakes combined with measured coseismic deformation from the 2001 event and the slip-rate yield an average return time for a large event close to 500 years [*Klinger et al.*, 2015]. Hence, the Kunlun earthquake occurred at a time when one could expect that the adjacent segment was already partially tectonically loaded, although not necessarily yet on the verge of failure.

Detailed mapping of the surface rupture related to the 2001 earthquake at the branching location (Figures 11.6 and 11.7) reveals a complex pattern of rupture. Overall, the rupture appears continuous across the branching section. The rupture, however, which is rather linear along the Kusai section, becomes more segmented with several right-stepping jogs generating local small compressional features as it approaches the junction. Eventually, once the rupture has propagated through the junction and continues along the Kunlun Pass fault, the surface rupture pattern gets back to a simpler linear surface expression (Figure 11.6). At the junction location, the main rupture trace bounds to the south the area affected by cracks. No significant ground rupture can be observed directly south of the main surface rupture. Only a few extensional cracks are documented several kilometers south from the main rupture, which are associated with the super-shear rupture propagation [*Bhat et al.*, 2007] and are not directly related to the branching process. Conversely, the area, about 500 m wide and located directly north of the main rupture trace, appears to be extensively affected (Figure 11.7) by a set of cracks that become more and more oblique to the main rupture trace as one moves eastward. The intensely damaged section is about 5.5 km long, starting from the place where the rupture begins to depart from the main Kusai section trace, right stepping toward the Kunlun Pass fault, to end where a well-established Kunlun Pass fault runs southward from the Xidatan section, about 1.2 km south of it. Actual sense of motion for individual cracks is not easy to determine, for each crack bears only a small amount of displacement. Most of the cracks, however, seem to accommodate at least a minor component of vertical deformation, while horizontal component is harder to recognize. The cracks are grossly parallel, aligned along a direction close to the local azimuth of the Xidatan section. The length of the cracks, which could also probably be called branches, varies from few meters to almost one kilometer for the longest. Such rupture pattern suggests that when the rupture arrived at the junction, probably at super-shear speed [*Vallee et al.*, 2008], the rupture attempted to breach toward the Xidatan segment. However, the triggering of the rupture along the western termination of the Xidatan section seems to have been hindered, probably by the presence of a strong asperity, while at the same time branching of the rupture along the Kunlun Pass fault was promoted by a low angle between the branch and the main fault, a close direction (<25°) of principal horizontal stress with the local fault azimuth, and a super-shear rupture [*Kame et al.*, 2003]. As the rupture fully developed along the Kunlun Pass fault, quickly the Xidatan section was in the shadow zone of the propagating rupture and could not rupture anymore. Hence, in the case of the Kunlun earthquake, both the specific geometry of the branch (low angle with the main fault) and the horizontal stress direction appear to have been key in promoting branching in

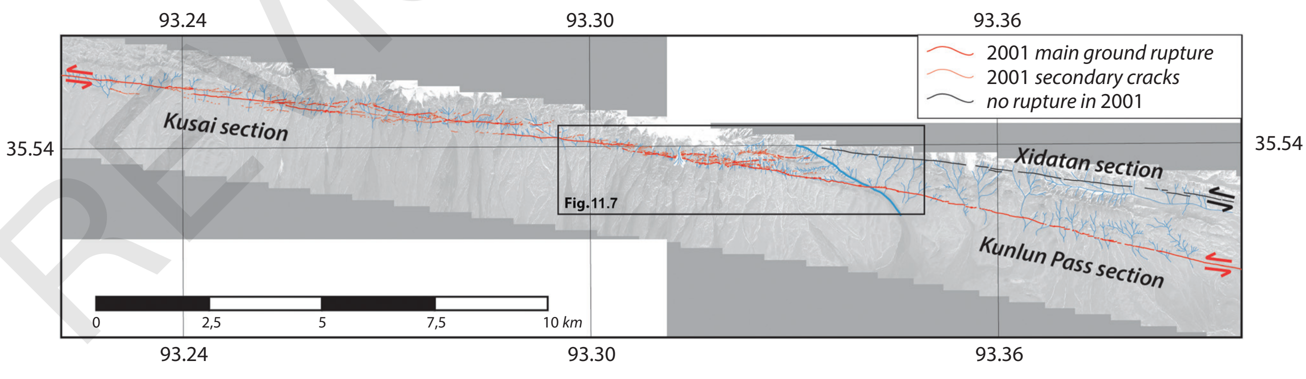

Figure 11.6 Detail from Figure 11.5. Junction between the Kusai section, to the west, the Xidatan section, long-term continuation of the Kunlun fault, and the Kunlun Pass fault. The rupture progressively jumped southward as it was moving eastward. Long-term morphology suggests that the rupture was following the path already used by previous earthquakes. Metric-resolution satellite image in background gives some sense of topography. Almost all drainages, including the major drainage at the junction between Xidatan and Kusai sections, flow south. *See electronic version for color representation*.

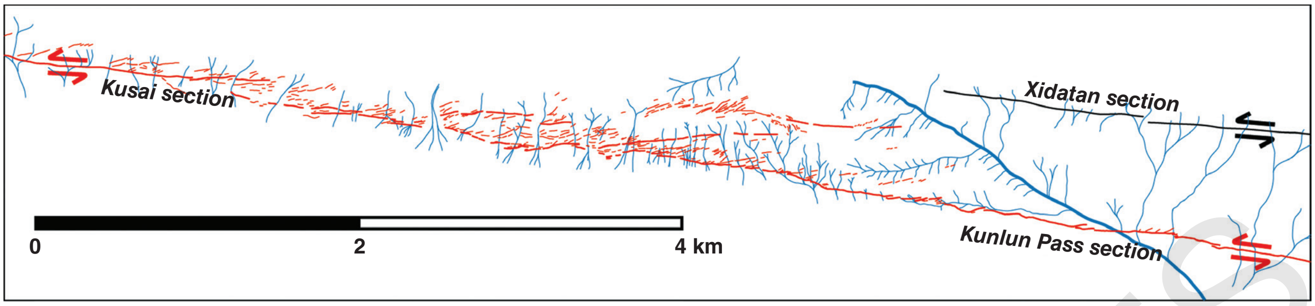

Figure 11.7 Detail of the zone in Figure 11.6 where the rupture branched off on the Kunlun Pass fault, instead of rupturing the Xidatan section. Numerous cracks north of the main rupture trace attest that the rupture tried to connect to the Xidatan section. Interestingly, almost no cracks are visible south of the main rupture. *See electronic version for color representation*.

the compressional quadrant, when in most configurations it is easier to promote rupture in the extensional quadrant [*Kame et al.*, 2003]. In the case of the 2001 event, super-shear rupture velocity made this configuration even more favorable for such branching.

Interestingly, the Kunlun fault is characterized by distinctive morphology along most of its length, which attests to its long-term activity and makes it easily identifiable in the landscape [*Li et al.*, 2005; *Klinger et al.*, 2015]. Similarly, although cumulative offsets are smaller, the western end of the Kunlun Pass branch is also characterized by evidence for long-term activity and a significant imprint in the landscape. At the junction between the proper Kunlun fault and the Kunlun Pass fault, however, the morphology is more confused. Anywhere else, the Kunlun fault is usually characterized by some linear topographic features such as ridge, valley, or fault scarp aligned with the fault direction, that crosscut the general morphology associated with the Kunlun Range, grossly controlled by the regional north-south drainage direction. The location of the junction, instead, is characterized by some positive topography with no clear evidence for a throughgoing fault, and an oblique river channel flowing south across the range (Figures 11.6 and 11.7). The channel does not show any obvious evidence of long-term left-lateral offset, as should be expected if earthquake ruptures would regularly offset the channel. Eventually, it suggests that earthquake ruptures propagating eastward along the Kusai section might never fully break through this asperity to connect to the Xidatan section. Instead, due to geometry and stress condition, the rupture would just stop at the junction or might branch to the Kunlun Pass Fault. The effect would be even more enhanced when super-shear propagation occurs. The positive topography visible at the junction site would then be associated with compressional deformation related to the right stepping of the rupture, accommodated by a myriad of cracks in the jog area. Hence, such a scenario would imply that earthquakes rupturing the Xidatan segment would either initiate at the junction and propagate eastward, or if propagating from the east, they would systematically end at the junction. Because some deformation is accommodated at the pressure ridge, and because the Xidatan fault and the Kunlun Pass fault run almost parallel for some distance, allowing for a progressive transfer of deformation, no long-term slip deficit should be expected at the junction between the two faults. The exact nature of structural connection, including at depth, between the Kusai segment and the Xidatan segment might, however, be more complex than previously thought and would deserve further investigation.

11.3. DISCUSSION

In the last decade, significant efforts have been made to try to improve earthquake hazard assessment in the framework of national or international consortiums, such as the Uniform California Earthquake Rupture Forecast project [*Field et al.*, 2014] or the Global Earthquake Model project (http://www.globalquakemodel.org/gem/). The main emphasis, for aspects directly related to geology, is on compiling accurate fault maps and the most complete earthquake record, including paleoseismicity, for each fault system considered. The way to incorporate fault geometry and possibilities for a rupture to jump from one fault to the next one, or to trigger rupture on a secondary fault, are at the core of the most recent developments of such projects and are highly debated in the literature [*Liu and Duan*, 2015; *Mignan et al.*, 2015].

Fault branches are first-order features when it comes to characterizing fault geometry. Careful examination of earthquake ruptures during the last century, when acceptable quality rupture maps are available, shows that in the majority of strike-slip cases, a major branch is involved. In some cases the epicenter or the end of the rupture is co-located with the junction between the main fault and the branch, such as in the case of the Bolnay earthquake discussed earlier in this chapter, or the Mw 7.1 Hector Mine earthquake in 1999 [*Jónsson et al.*, 2002].

More interestingly, the rupture often branches off the main fault during propagation to end up in a cul-de-sac, where it dies out, stopping the earthquake. This is the case, for example, with the earthquakes of Denali or Kunlun, extensively discussed earlier in this chapter, but it has been documented for many other large earthquakes such as the Mw 7.9 1939 Erzincan earthquake along the North Anatolian fault, Turkey [*Barka*, 1996]; the Mw 7.2 Izmit/Mw 7.1 Ducze earthquake sequence in 1999, also along the North Anatolian fault [*Rockwell et al.*, 2002]; or the Mw 7.9 Manyi earthquake in Tibet [*Peltzer et al.*, 1999], to name only a few. In several cases, although the branch could be identified in the landform morphology even before the most recent earthquake took place, a well-developed connection between the main fault and the branch was not always easy to recognize, if existing at all. In fact, in the case of strike-slip motion, the location where a branch connects to the main fault is similar to a triple junction between three strike-slip faults and, as such, should not be expected to be stable through time [*McKenzie and Morgan*, 1969], possibly hindering development of a clear morphological signature. At short timescale, stress-shadowing effects during an individual rupture might also come into play to prevent concomitant rupturing and further connection of the three legs of the fault junction [*Ando et al.*, 2009].

Identification of such structures, understanding of their impact on rupture propagation, and incorporation of such knowledge in earthquake rupture scenario might, however, prove to be efficient in limiting the number of possible rupture scenarios to test while assessing seismic hazard for large regions. The example of the Kunlun rupture suggests that in that case, any rupture that would propagate eastward along the Kusai section might branch and die on the Kunlun Pass fault. Similarly, our observations suggest that rupture along the Xidatan section would either initiate or end at the junction but not go through this junction. Hence, such considerations limit the number of potential rupture scenarios along this part of the Kunlun fault, as well as the size of potential earthquakes. Similar factors have been taken into account in considering the following: various rupture scenarios along the Marmara Sea section of the North Anatolian fault [*Oglesby et al.*, 2008], possibilities of simultaneous ruptures of the southern section of the San Andreas fault and of the San Jacinto fault [*Lozos et al.*, 2012; *Lozos*, 2016], and rupture extent along the Altyn Tagh fault [*Elliott et al.*, 2015].

Eventually, it appears from case studies that fault branching is a major player in the propagation and arrest of, at the minimum, strike-slip ruptures. It is likely that branches would also be important during propagation of dip-slip ruptures [*Templeton et al.*, 2010; *Melnick et al.*, 2012; *Xu et al.*, 2015].

A significant effort in developing conceptual models and efficient modeling tools has been emerging in the last decades to account for such complex geometry. Taking advantage of the increase in computational capabilities, models including dynamic rupture propagation on multiple planar vertical fault planes embedded in a volume have been developed that give us some new insight into dynamic fault interaction, including fault branching [*Oglesby et al.*, 2008; *Lozos*, 2016]. Planar nonvertical faults have also been modeled to look at geometry effects for dip-slip faults, such as the thrust fault that caused the Mw 7.7 Chi-Chi earthquake in Taiwan in 1999 [*Oglesby and Day*, 2001]. Recent work explored possibilities of models including nonplanar faults [*Duru and Dunham*, 2016], which show the impact of fault roughness on wave propagation and deformation patterns [*Bruhat et al.*, 2016].

Eventually, these different approaches will converge to provide the community with some tools able to incorporate field data with a level of detail similar to what is presented in this chapter. Based on real case studies, we might then be able to better understand what actually controls rupture branching and to focus only on the most likely rupture schemes when running earthquake scenario for an entire fault system.

ACKNOWLEDGMENTS

This work was partly funded by ANR Geosmec contract ANR-12-BS06-0016 and by a grant from the city of Paris. We thank the editor, M. Thomas, and two anonymous reviewers for insightful comments and suggestions that significantly improved this manuscript.

REFERENCES

Ando, R., B. E. Shaw, and C. H. Scholz (2009), Quantifying natural fault geometry: Statistics of splay fault angles, *Bulletin of the Seismological Society of America*, *99*(1), 389–395, doi:10.1785/0120080942.

Baljinnyam, I., *et al.* (1993), Ruptures of major earthquakes and active deformation in Mongolia and its surroundings, *Geological Society of America Memoir 181*, 62 pp., The Geological Society of America, Boulder.

Barka, A. (1996), Slip distribution along the North Anatolian fault associated with the large earthquakes of the period 1939–1967, *Bull. Seism. Soc. Am.*, *86*(5), 1238–1254.

Bhat, H. S., R. Dmowska, G. C. P. King, Y. Klinger, and J. R. Rice (2007), Off-fault damage patterns due to supershear ruptures with application to the 2001 M-w 8.1 Kokoxili (Kunlun) Tibet earthquake, *Journal of Geophysical Research: Solid Earth*, *112*, B06301, doi:10.1029/2006JB004425.

Bhat, H., R. Dmowska, J. Rice, and N. Kame (2004), Dynamic slip transfer from the Denali to Totschunda faults, Alaska: Testing theory for fault branching, *Bulletin of the Seismological Society of America*, *94*(6B), S202–S213.

Bouchon, M., and M. Vallée (2003), Observation of long supershear rupture during the Ms = 8.1 Kunlunshan earthquake, *Science*, *301*(5634), 824–826.

Bruhat, L., Z. Fang, and E. M. Dunham (2016), Rupture complexity and the supershear transition on rough faults, *Journal of Geophysical Research: Solid Earth*, *121*, doi :10.1002/2015JB012512

Chéry, J., S. Carretier, and J.-F. Ritz (2001), Postseismic stress transfer explains time clustering of large earthquakes in Mongolia, *Earth and Planetary Science Letters*, *194*(1), 277–286.

Choi, J.-H., *et al.* (2015), High-resolution surface-rupture map and slip distribution for the 1905 M8 Tsetserleg-Bulnay, Mongolia, earthquake sequence, paper presented at AGU Fall meeting, San Francisco CA, USA, 14–18 December.

Dreger, D. S., D. D. Oglesby, R. Harris, N. Ratchkovski, and R. Hansen (2004), Kinematic and dynamic rupture models of the November 3, 2002 Mw7. 9 Denali, Alaska, earthquake, *Geophysical Research Letters*, *31*(4).

Duan, B., and D. D. Oglesby (2006), Heterogeneous fault stresses from previous earthquakes and the effect on dynamics of parallel strike-slip faults, *Journal of Geophysical Research*, *111*, B05309, doi:10.1029/2005JB004138.

Dunham, E. M., and R. J. Archuleta (2004), Evidence for a supershear transient during the 2002 Denali fault earthquake, *Bulletin of the Seismological Society of America*, *94*(6B), S256–S268.

Duru, K., and E. M. Dunham (2016), Dynamic earthquake rupture simulations on nonplanar faults embedded in 3D geometrically complex, heterogeneous elastic solids, *Journal of Computational Physics*, *305*, 185–207.

Elliott, A. J., M. E. Oskin, J. Liu-Zeng, and Y. Shao (2015), Rupture termination at restraining bends: The last great earthquake on the Altyn Tagh Fault, *Geophysical Research Letters*, *42*(7), 2164–2170.

Elliott, J. L., C. F. Larsen, J. T. Freymueller, and R. J. Motyka (2010), Tectonic block motion and glacial isostatic adjustment in southeast Alaska and adjacent Canada constrained by GPS measurements, *Journal of Geophysical Research: Solid Earth (1978–2012)*, *115*(B9).

Field, E. H., R. J. Arrowsmith, G. P. Biasi, P. Bird, T. E. Dawson, K. R. Felzer, D. D. Jackson, K. M. Johnson, T. H. Jordan, and C. Madden (2014), Uniform California Earthquake Rupture Forecast, Version 3 (UCERF3): The time-independent model, *Bulletin of the Seismological Society of America*, *104*(3), 1122–1180.

Haeussler, P. J., *et al.* (2004), Surface rupture and slip distribution of the Denali and Totschunda faults in the 3 November 2002 M 7.9 earthquake, *Alaska, Bulletin of the Seismological Society of America*, *94*(6), S23–S52.

Harris, R., and S. Day (1993), Dynamics of fault interaction: Parallel strike-slip faults, *J. Geophys. Res.*, *98*(B3), 4461–4472.

Harris, R., and S. Day (1999), Dynamic 3D simulations of earthquakes on en echelon faults, *Geophys. Res. Lett.*, *26*(14), 2089–2092.

Ji, C., R. J. Archuleta, and C. Twardzik (2015), Rupture history of 2014 Mw 6.0 South Napa earthquake inferred from near-fault strong motion data and its impact to the practice of ground strong motion prediction, *Geophysical Research Letters*, *42*(7), 2149–2156.

Jónsson, S., H. Zebker, P. Segall, and F. Amelung (2002), Fault slip distribution of the 1999 Mw 7.1 Hector Mine, California, earthquake, estimated from satellite radar and GPS measurements, *Bulletin of the Seismological Society of America*, *92*(4), 1377–1389.

Kame, N., J. R. Rice, and R. Dmowska (2003), Effects of prestress state and rupture velocity on dynamic fault branching, *J. Geophys. Res.*, *108*(B5), 2265, doi:10.1029/2002JB002189.

Khilko, S., R. Kurushin, V. Kotchetkov, L. Misharina, V. Melnikova, N. Gileva, S. Lastochkin, I. Baljinnyam, and D. Monhoo (1985), Earthquakes and the base of the seismogenic zoning of Mongolia, *Joint Soviet-Mongolian Research Geological Scientific Expedition*, *41*, 225.

Kim, A., and D. S. Dreger (2008), Rupture process of the 2004 Parkfield earthquake from near-fault seismic waveform and geodetic records, *Journal of Geophysical Research: Solid Earth*, *113*(B7).

King, G., Y. Klinger, D. Bowman, and P. Tapponnier (2005), Slip partitioned surface breaks for the 2001 Kokoxili earthquake, China (Mw 7.8), *Bull. Seis. Soc. Am*, *95*(2), 731–738.

King, G. C., and J. Nabelek (1985), The role of fault bends in faults in the initiation and termination of earthquake rupture, *Science*, *283*, 984–987.

Klinger, Y. (2010), Relation between continental strike-slip earthquake segmentation and thickness of the crust, *J. Geophys. Res.*, *115*, doi:10.1029/2009JB006550.

Klinger, Y., M. Etchebes, P. Tapponnier, and C. Narteau (2011), Characteristic slip for five great earthquakes along the Fuyun fault in China, *Nature Geoscience*, *4*(6), 389–392, doi:10.1038/ngeo1158.

Klinger, Y., R. Michel, and G. C. P. King (2006), Evidence for an earthquake barrier model from Mw similar to 7.8 Kokoxili (Tibet) earthquake slip-distribution, *Earth and Planetary Science Letters*, *242*(3-4), 354–364.

Klinger, Y., X. Xu, G. Chen, J. Van Der Woerd, J. Liu-Zeng, and J. M. Nocquet (2015), Fault segmentation and earthquake history of the Kunlun fault, China, paper presented at AGU Fall meeting, San Francisco CA, USA, 14–18 December.

Klinger, Y., X. W. Xu, P. Tapponnier, J. Van der Woerd, C. Lasserre, and G. King (2005), High-resolution satellite imagery mapping of the surface rupture and slip distribution of the MW 7.8, 14 November 2001 Kokoxili Earthquake, Kunlun Fault, northern Tibet, China, *Bull. Seis. Soc. Am.*, *95*(5), 1970–1987.

Lettis, W., J. Bachhuber, A. Barka, R. Witter, and C. Brankman (Eds.) (2000), Surface fault rupture and segmentation during the Kocaeli earthquake, Istanbul Technical University, Istanbul.

Li, H. B., J. Van der Woerd, P. Tapponnier, Y. Klinger, X. X. Qi, J. S. Yang, and Y. T. Zhu (2005), Slip rate on the Kunlun fault at Hongshui Gou, and recurrence time of great events comparable to the 14/11/2001, Mw similar to 7.9 Kokoxili earthquake, Earth and Planetary Science Letters, *237*(1-2), 285–299.

Lin, A. M., J. M. Guo, K. Kano, and Y. Awata (2006), Average slip rate and recurrence interval of large-magnitude earthquakes on the western segment of the strike-slip Kunlun fault, northern Tibet, *Bulletin of the Seismological Society of America*, *96*, 1597–1611, doi:10.1785/0120050051.

Liu, Z., and B. Duan (2015), Coseismic Slip Gradient and Rupture Jumps on Parallel Strike-Slip Faults, *Bulletin of the Seismological Society of America*.

Lozos, J. C. (2016), A case for historic joint rupture of the San Andreas and San Jacinto faults, *Science Advances*, *2*(3), e1500621.

Lozos, J. C., D. D. Oglesby, J. N. Brune, and K. B. Olsen (2012), Small intermediate fault segments can either aid or hinder rupture propagation at stepovers, *Geophysical Research Letters*, *39*(18).

Manighetti, I., G. C. P. King, and C. G. Sammis (2004), The role of off-fault damage in the evolution of normal faults, *Earth and Planetary Science Letters*, *217*, 399–408.

Marechal, A. (2015), Tectonique active de la zone de collision Yakutat–Nord Amérique: Apport du GPS et de la géomorphologie à l'étude de la partition de la déformation, Université Montpellier.

Marechal, A., S. Mazzotti, J. L. Elliot, J. T. Freymueller, and M. Schmidt (2015), Indentor-corner tectonics in the Yakutat-St. Elias collision constrained by GPS, *Journal of Geophysical Research: Solid Earth*, *120*(5), 3897–3908.

Massonnet, D., M. Rossi, C. Carmona, F. Adragna, G. Peltzer, K. Feigl, and T. Rabaute (1993), The displacement field of the Landers earthquake mapped by radar interferometry, *Nature*, *364*(6433), 138–141.

Matmon, A., D. Schwartz, P. J. Haeussler, R. Finkel, J. Lienkaemper, H. Stenner, and T. Dawson (2006), Denali fault slip rates and Holocene–late Pleistocene kinematics of central Alaska, *Geology*, *34*(8), 645–648.

McKenzie, D., and W. J. Morgan (1969), Evolution of triple junctions, *Nature*, *224*, 125–133.

Melnick, D., M. Moreno, M. Motagh, M. Cisternas, and R. L. Wesson (2012), Splay fault slip during the Mw 8.8 2010 Maule Chile earthquake, *Geology*, *40*(3), 251–254.

Mériaux, A. S., K. Sieh, R. C. Finkel, C. M. Rubin, M. H. Taylor, A. J. Meltzner, and F. J. Ryerson (2009), Kinematic behavior of southern Alaska constrained by westward decreasing postglacial slip rates on the Denali Fault, Alaska, *Journal of Geophysical Research: Solid Earth (1978–2012)*, *114*(B3).

Mignan, A., L. Danciu, and D. Giardini (2015), Reassessment of the maximum fault rupture length of strike-slip earthquakes and inference on Mmax in the Anatolian Peninsula, Turkey, *Seismological Research Letters*, *86*(3), 890–900.

Muller, J. R., and A. Aydin (2004), Rupture progression along discontinuous oblique fault sets: Implications for the Karadere rupture segment of the 1999 Izmit earthquake, and future rupture in the Sea of Marmara, *Tectonophysics*, *391*(1), 283–302.

Nielsen, S., and L. Knopoff (1998), The equivalent strength of geometrical barriers to earthquakes, *Journal of Geophysical Research*, *103*(B5), 9953–9965.

Oglesby, D., M. Mai, K. Atakan, and S. Pucci (2008), Dynamic models of earthquakes on the North Anatolian fault zone under the Sea of Marmara: Effect of hypocenter location, *Geophys. Res. Let.*, *35*, doi:10.1029/2008GL035037.

Oglesby, D. D., and S. M. Day (2001), The effect of fault geometry on the 1999 Chi-Chi (Taiwan) earthquake, *Geophysical Research Letters*, *28*(9), 1831–1834.

Oskin, M. E., *et al.* (2012), Near-field deformation from the El Mayor-Cucapah earthquake revealed by differential LIDAR, *Science*, *335*(6069), 702–705, doi:10.1126/science.1213778.

Peltzer, G., F. Crampe, and G. King (1999), Evidence of nonlinear elasticity of the crust from the Mw7.6 Manyi (Tibet) earthquake, *Science*, *286*(8 October 1999), 272–276.

Poliakov, A. N., R. Dmowska, and J. R. Rice (2002), Dynamic shear rupture interactions with fault bends and off-axis secondary faulting, *Journal of Geophysical Research*, *107*(B11), 6–18, doi:10.1029/2001JB000572.

Ren, Z., Z. Zhang, T. Chen, S. Yan, J. Yin, P. Zhang, W. Zheng, H. Zhang, and C. Li (2016), Clustering of offsets on the Haiyuan fault and their relationship to paleoearthquakes, *Geological Society of America Bulletin*, *128*(1-2), 3–18.

Rizza, M., J. F. Ritz, C. Prentice, R. Vassallo, R. Braucher, C. Larroque, A. Arzhannikova, S. Arzhannikov, S. Mahan, and M. Massault (2015), Earthquake geology of the Bulnay Fault (Mongolia), *Bulletin of the Seismological Society of America*, *105*(1), 72–93.

Rockwell, T., S. Lindvall, T. Dawson, R. Langridge, W. Lettis, and Y. Klinger (2002), Lateral offsets on surveyed cultural features resulting from the 1999 Izmit and Duzce earthquakes, Turkey, Bulletin Seismological Society America, *92*, 79–94.

Schlupp, A., and A. Cisternas (2007), Source history of the 1905 great Mongolian earthquakes (Tsetserleg, Bolnay), *Geophysical Journal International*, *169*(3), 1115–1131.

Schwartz, D. P., H. Haessler, G. G. Seitz, and T. E. Dawson (2012), Why the 2002 Denali fault rupture propagated onto the Totschunda fault: Implication for fault branching and seismic hazards, *Journal of Geophysical Research: Solid Earth*, *117*, B11304, doi:10.1029/2011JB008918.

Sieh, K., *et al.* (1993), Near-field investigations of the Landers earthquake sequence, April to July 1992, *Science*, *260*(5105), 171–176.

Spotila, J. A., and A. L. Berger (2010), Exhumation at orogenic indentor corners under long- term glacial conditions: Example of the St. Elias orogen, southern Alaska, *Tectonophysics*, *490*(3-4), 241–256.

Tapponnier, P., and P. Molnar (1977), Active faulting and tectonics in China, *Journal of Geophysical Research*, *82*, 2905–2930.

Tapponnier, P., X. Zhiqin, F. Roger, B. Meyer, N. Arnaud, G. Wittlinger, and Y. Jingsui (2001), Oblique stepwise rise and growth of the Tibet plateau, *Science*, *294*, 1671–1677.

Templeton, E. L., H. Bhat, R. Dmowska, and J. Rice (2010), Dynamic rupture through branched fault configuration at Yucca Mountain and resulting ground motions, *Bul. Seis. Soc. Am.*, *100*(4), 1485–1497.

Teran, O. J., J. M. Fletcher, M. E. Oskin, T. K. Rockwell, K. W. Hudnut, R. M. Spelz, S. O. Akciz, A. P. Hernandez-Flores, and A. E. Morelan (2015), Geologic and structural controls on rupture zone fabric: A field-based study of the 2010 Mw 7.2 El Mayor–Cucapah earthquake surface rupture, *Geosphere*, *11*(3), 899–920.

Thomas, M., H. S. Bhat, and Y. Klinger (2017), Effect of brittle off-fault damage on earthquake rupture dynamics, in *Fault zone dynamic processes: Evolution of fault properties during seismic rupture*, edited by M. Y. Thomas, T. M. Mitchell, and H. S. Bhat, AGU/Wiley.

Vallage, A., M. H. Devès, Y. Klinger, G. C. P. King, and N. A. Ruppert (2014), Localized slip and distributed deformation in oblique settings: The example of the Denali fault system, Alaska, *Geophysical Journal International*, *197*(3), 1284–1298.

Vallage, A., Y. Klinger, R. Grandin, H. S. Bhat, and M. Pierrot-Deseilligny (2015), Inelastic surface deformation during the 2013 Mw7.7 Balochistan, Pakistan, earthquake, *Geology*, *43*(12), 1079–1082, doi:10.1130/G37290.1.

Vallee, M., M. Landès, N. M. Shapiro, and Y. Klinger (2008), The 14 November 2001 Kokoxili (Tibet) earthquake: High-frequency seismic radiation originating from the transition between sub-Rayleigh and supershear rupture velocity regimes, *Journal of Geophysical Research*, *113*, B07305, doi:10.1029/2007JB005520.

Van Der Woerd, J., F. J. Ryerson, P. Tapponnier, A. S. Meriaux, Y. Gaudemer, B. Meyer, R. Finkel, M. Caffee, G. Zhao, and Z. Xu (2000), Uniform slip-rate along the Kunlun fault: Implication for seismic behaviour and large-scale tectonics, *Geophys. Res. Lett.*, *27*, 2353–2356.

Van Der Woerd, J., P. Tapponnier, F. J. Ryerson, A. S. Meriaux, B. Meyer, Y. Gaudemer, R. C. Finkel, M. W. Caffee, G. G. Zhao, and Z. Q. Xu (2002), Uniform postglacial slip-rate along the central 600 km of the Kunlun Fault (Tibet), from Al-26, Be-10, and C-14 dating of riser offsets, and climatic origin of the regional morphology, *Geophysical Journal International*, *148*(3), 356–388.

Wang, Q., *et al.* (2001), Present-day crustal deformation in China constrained by global positioning system measurements, *Science*, *294*, 574–577.

Wei, S., *et al.* (2011), Surficial simplicity of the 2010 El Mayor-Cucapah earthquake of Baja California in Mexico, *Nature Geoscience*, *4*, 615–618, doi:10.1038/NGEO1213.

Wesnousky, S. (2006), Predicting the endpoints of earthquake ruptures, *Nature*, *444*(7117), 358–360.

Wesnousky, S. (2008), Displacement and geometrical characteristics of earthquake surface ruptures: Issues and implications for seismic-hazard analysis and the process of earthquake rupture, *Bull. Seis. Soc. Am.*, *98*(4), 1609–1632, doi:10.1785/0120070111.

Xu, S., E. Fukuyama, Y. Ben-Zion, and J.-P. Ampuero (2015), Dynamic rupture activation of backthrust fault branching, *Tectonophysics*, *644*, 161–183.

Xu, X. W., G. H. Yu, Y. Klinger, P. Tapponnier, and J. Van der Woerd (2006), Reevaluation of surface rupture parameters and faulting segmentation of the 2001 Kunlunshan earthquake (M(w)7.8), northern Tibetan Plateau, China, *J. Geophys. Res.*, *111*(B5), B05316, doi:10.1029/2004JB003488.